IEEE Journal of Oceanic Engineering, Vol. 45, No. 4, 2020

Underwater Position and Attitude Estimation Using Acoustic, Inertial, and Depth Measurements

Erlend Kvinge Jørgensen, Thor I. Fossen, Torleiv H. Bryne, and Ingrid Schjølberg

***Abstract*—This article considers the problem of constructing an observer for estimating position, velocity, attitude, underwater wave speed, rate sensor bias, and accelerometer bias that has both proven stability and close-to-optimal performance with respect to noise. The observer takes pseudorange, pseudorange difference, depth, and inertial measurements as input, and has a cascade structure for which the equilibrium point is proven to be locally exponentially stable due to the singularities in the attitude representation. The design of the observer is based on the exogenous Kalman filter principle, in which estimators with proven stability provide a linearization point for a linearized Kalman filter, to achieve both proven stability and close-to-optimal noise properties. Experimental validation is provided, with ground truth values generated by a camera positioning system with millimeter accuracy. The observer is compared to an extended Kalman filter and to a nonimplementable linearized Kalman filter using the true state as the linearization point, and the estimation error is almost identical to the linearized Kalman filter using the true state as a linearization point.**

***Index Terms*—Cascaded systems, exogenous Kalman filter (EKF), linearized Kalman filter (LKF), nonlinear filtering, state estimation.**

I. Introduction

ACCURATE and reliable state estimation is a central part in reaching the goal of autonomous underwater vehicles. A common approach for determining position underwater today is employing a long baseline (LBL) acoustic network, in which the time of arrival (TOA) of acoustic signals from several known fixed positions is measured. The TOA measurements relate directly to the distance, and these distances can be used to determine position. It is also common to use an inertial measurement unit (IMU), providing body-fixed measurements of specific force and angular rate. For determining attitude, a combination of specific force measurements and either a magnetometer or a gyrocompass measurement is most commonly used in addition to the body-fixed angular rate sensor. In previous work [1], [2], solutions where two or more acoustic receivers are placed on the vehicle have been suggested, in which difference-in-time-of-arrival (DTOA) measurements become available, and can be used as additional information for determining attitude more robustly. This approach will be further investigated in the following article. Similar approaches can be found for surface vehicles, in which several GPS antennas are placed on the vehicle, and the measurements are used to determine attitude [3], [4].

As mentioned above, it is possible to measure the body-fixed acceleration and angular rate using an IMU. However, these measurements are corrupted by both noise and biases. Consequently, it is not sufficient to simply integrate these measurements, and other measurements are needed to estimate the biases and to take noise into account as optimally as possible. For position, an LBL or an ultrashort baseline (USBL) system is usually employed to provide additional information to compensate for the uncertainties in the acceleration measurement. A review of range-based positioning can be found in [5]. Globally exponentially stable (GES) observers for underwater navigation using LBL measurements are suggested in [6] and [7], and a globally asymptotically stable (GAS) observer is suggested in [8]. More recent approaches are described in [9]–[11]. Some classical approaches for underwater navigation using LBL measurements can be found in [12]–[16].

For attitude, it is common to use two or more nonparallel reference vectors that are known in either body or inertial frame and measured in the other frame as additional measurements. These can be used to determine attitude [17]. For constant reference vectors, a nonlinear observer (NLO) for estimating attitude and rate sensor bias with global stability properties was suggested in [18], and extended to time-varying reference vectors in [19]. It is also common to use the multiplicative extended Kalman filter (EKF) for attitude estimation [20]. Other approaches for nonlinear attitude determination are suggested, for example, in [21] and [22], and a survey can be found in [23].

For accurate position estimation, it is central that the attitude estimate is as accurate as possible, especially the roll and pitch angle. The reason for this is that the specific force measurement needs to be rotated from the body frame to the inertial frame before the gravity vector is subtracted. As the measured acceleration from gravity is about an order of magnitude higher than the expected acceleration for an underwater vehicle, an inaccurate rotation will cause significant errors in the velocity and position estimate. When determining attitude using the specific force measurement along with a magnetometer or a gyrocompass measurement, the measured specific force is assumed to be the

This work was supported in part by the Norwegian University of Science and Technology Center of Autonomous Marine Operations and Systems under Grant 223254 and in part by the NextGenIMR under Grant 234108. This work was presented in part at Autonomous Underwater Vehicles 2016, Tokyo, Japan, November 6–9, 2016.

E. K. Jørgensen and I. Schjølberg are with the Department of Marine Technology, Norwegian University of Science and Technology, 7491 Trondheim, Norway (e-mail: erlend.k.jorgensen@ntnu.no; ingrid.schjolberg@ntnu.no).

T. I. Fossen and T. H. Bryne are with the Department of Engineering Cybernetics, Norwegian University of Science and Technology, 7491 Trondheim, Norway (e-mail: thor.fossen@ntnu.no; torleiv.h.bryne@ntnu.no).

gravity vector, and the magnetic field is assumed to be known beforehand. However, this approach has some drawbacks: The magnetometer is prone to both internal and external disturbances, and the gyrocompass is very accurate, but it is heavy, large, and expensive and requires recalibration. Furthermore, as mentioned above, the accelerometer measurement also has a bias, which will perturb the attitude estimate if not taken into account.

There are two ways of taking accelerometer bias into account, either by precalibration or online estimation. As the accelerometer bias is time varying, precalibration is only valid for a certain period of time, depending on the quality of the IMU. For online estimation, if the accelerometer is also used to determine roll and pitch angle, which is usually the case, a persistent excitation demand is put on the attitude, and very accurate measurements are required to be able to estimate the accelerometer bias accurately. This is due to the usage of the accelerometer measurement in both position and attitude estimation. Schemes for estimating accelerometer bias offline are suggested in [24] and [25], and online accelerometer bias estimation schemes are suggested in [24], [26], and [27].

By employing DTOA measurements, it is, as shown in [2], possible to estimate attitude using none of the accelerometer, magnetometer, and gyrocompass measurements. A similar approach can be found in [28], in which an NLO is proposed, based on a combination of LBL, USBL, and rate sensor measurements. This makes it possible to decouple the attitude estimation from the accelerometer measurement, removing the demand for large excitations of the system for online accelerometer bias estimation while increasing the accuracy of the accelerometer bias estimate, thus increasing the accuracy of the position estimate.

The goal of this article is to develop an observer with proven stability and close-to-optimal performance w.r.t. noise, for determining position, velocity, attitude (PVA), underwater acoustic wave speed (AWS), rate sensor bias, and accelerometer bias using TOA, DTOA, IMU, and depth measurements. Applying DTOA measurements can increase the accuracy of the attitude and accelerometer bias estimate, thus increasing the accuracy of the position estimate. This article builds on the work in [29] and [30], where an observer is suggested for determining position, velocity, and AWS using LBL and depth measurements. It also builds on the work in [2], where a locally exponentially stable (LES) observer with easily identifiable singular points is suggested, estimating attitude and rate sensor bias using only a position estimate and TDOA and rate sensor measurements, and [1], in which the accelerometer measurement is used to estimate roll and pitch. These two observers are used as parts of the proposed observer. Furthermore, the proposed observer relaxes the assumption made in [1], that accelerometer bias is known, by estimating accelerometer bias online, and an observer for determining a rough bias estimate used as a linearization point is suggested.

A. Exogenous Kalman Filter (XKF)

The suggested observer is based on the XKF principle. The XKF is a filter design principle proposed in [31] in which an auxiliary estimator with proven stability provides a linearization point for a linearized Kalman filter (LKF). The motivation for this principle is to get an estimation scheme for nonlinear systems that has both proven stability and close-to-optimal noise properties. Kalman filters (KFs) with a previous algebraic transformation and NLOs have proven stability but not close-to-optimal noise properties, whereas, for example, the particle filter usually has close-to-optimal noise properties but not proven stability. Furthermore, the EKF also usually has close-to-optimal noise properties, but rarely has proven stability. As stated in [31], if the auxiliary estimator has proven stability, and the model for the LKF satisfies certain criteria, the LKF will inherit the stability properties of the auxiliary estimator, whereas also in most cases, depending on the accuracy of the auxiliary estimator, it will give estimates with close-to-optimal noise properties. The accuracy required by the auxiliary estimator to yield the output of the filter close-to-optimal is system dependent, especially with regard to the degree of nonlinearity in the system model.

The computational complexity of the XKF is naturally larger than for the EKF, as an auxiliary estimator is needed. However, it is significantly lower than other common nonlinear estimation approaches, such as the particle filter and the unscented Kalman filter. For more examples of the XKF, see [29] and [32]. For more details about particle filters and EKF, see, for example, [33] and [34], and for more details regarding NLOs, see, for example, [35].

B. Main Contribution

The main contributions of this article are as follows.

Theorem 1, the equilibrium point of a cascaded observer for estimating PVA, AWS, and rate sensor bias while also estimating accelerometer bias online, is proven to be LES with known singularity points. The latter is achieved without any conditions of the motion of the vehicle. The cascade consists partly of subsystems investigated in previous papers, and lemmas stating stability of the cascades of these subsystems are presented. Furthermore, experiments suggest that the observer also has close-to-optimal noise properties.

A second contribution is experimental validation of the observer, provided from tests performed in MCLab, a lab testing facility at the Norwegian University of Science and Technology, Trondheim, Norway. The observer is compared to an EKF and a nonimplementable optimal LKF to validate the claim that the observer has close-to-optimal stationary performance, and similar stationary performance as the EKF. Due to the presence of ground truth measurements, the performance of the observer, along with the relative performance of all estimators, can be evaluated accurately. Furthermore, implementation aspects and practical issues are discussed, and solutions to these issues are proposed.

C. Outline

This article is organized as follows. Section II describes the system and measurement models. Section III shows the overall structure of the observer and presents the theoretical results. Section IV discusses the practical aspects, regarding system

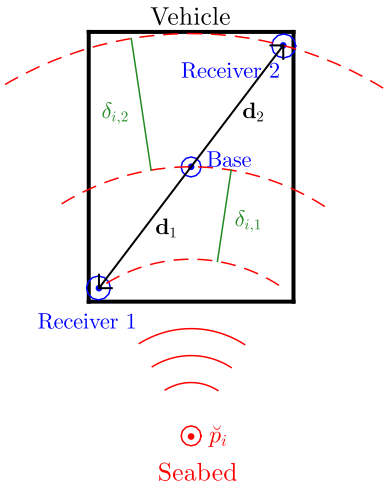

Fig. 1. Illustration of system with range-difference measurements. Variables are defined and explained in Section II-C [1]

setup, calibration of equipment, and implementation of the observer. Section V provides the results from the lab experiments. Section VI gives a short discussion regarding the results and possible improvement of the system. Section VII contains the conclusion.

II. System and Measurement Models

In this section, the system and measurements used will be described. Furthermore, an algebraic transform is performed in one of the steps in the observer. This transformation is also described in detail.

A. Acoustic System Description

The acoustic system consists of $N \geq 3$ senders and $M+1 \geq 3$ receivers. The senders are placed on the sea bottom with known fixed positions in the global frame, and the receivers are placed on the vehicle with known fixed positions in the body frame. One receiver is chosen as the "base" receiver, and the vectors between this receiver and the other receivers are denoted by $\mathbf{d}_{1,\ldots,M}$. A signal is sent simultaneously from each sender, and from measuring the difference in time it takes for a signal to reach each receiver, information about the attitude can be extracted. An illustration of the system is shown in Fig. 1, and the requirements for the geometry of the senders and receivers are stated as assumptions in Section II-C.

B. Attitude Representation

In the suggested observer, the attitude is represented with Euler angles, and, more specifically, the common roll–pitch–yaw convention where $\mathbf{\Theta} = [\psi, \theta, \phi]^T$ and $\mathbf{R}_b^n(\mathbf{\Theta}) = \mathbf{R}_z(\psi)\mathbf{R}_y(\theta)\mathbf{R}_x(\phi)$. It is known that this representation has singularities in the dynamic model when the pitch angle reaches $\theta = \pi/2 + k\pi,\ k \in \mathbb{Z}$. However, these pitch angles are very uncommon for most underwater vehicles used today. Furthermore, the singularities are known, and it is possible to change the Euler angle representation to a representation with different singularities if the system detects that the vehicle is approaching one of the singularities [35]. Alternatively, unit quaternions can be used [36]. However, the stability analysis is also fairly straightforward for Euler angles, as it is a very intuitive representation, and is not a redundant representation such as, for example, quaternions, thus omitting the need for more extensive stability proofs involving coordinate transformations reducing the degrees of freedom.

C. Measurement Models

The two coordinate frames used in this article are the body frame and the north-east-down (NED) frame, approximated as a local inertial frame with origin defined by the Qualisys camera system. The Qualisys system is used for providing ground truth information, described in more detail in Section IV-A.

The IMU in the experiment is fixed on the vehicle, known as a strapdown system. Consequently, the measurements from the IMU are in the body frame. The measurements used in the suggested observer are acceleration and angular rate, modeled as

$$\begin{aligned}\mathbf{a}_{\text{imu}}^b &= \mathbf{a}^b - \mathbf{R}_n^b \mathbf{g}^n + \mathbf{b}_a + \epsilon_a \\ &= \mathbf{R}_n^b(\mathbf{a}^n - \mathbf{g}^n) + \mathbf{b}_a + \epsilon_a \qquad (1)\end{aligned}$$

$$\boldsymbol{\omega}_{\text{imu}}^b = \boldsymbol{\omega}_{b/n}^b + \mathbf{b}_\omega + \epsilon_\omega \qquad (2)$$

where $\mathbf{a}^b$ and $\mathbf{a}^n$ are the vehicle acceleration in the body and NED coordinate frame subsequently, $\mathbf{g}^n$ is the gravity vector in the NED frame, $\mathbf{R}_n^b$ is the rotation matrix from the NED frame to the body frame, $\mathbf{b}_a$ is a slowly time-varying acceleration measurement bias, $\boldsymbol{\omega}_{b/n}^b$ is the angular rate of the body frame relative to the NED frame, expressed in the body frame, $\mathbf{b}_\omega$ is a slowly time-varying rate sensor bias, and ϵ_a and ϵ_ω are zero-mean Gaussian white noise vectors with covariances $\mathbf{Q}_a$ and $\mathbf{Q}_\omega$.

The TOA measurements are modeled as pseudoranges, ranges affected by an unknown parameter. The model is based on the formulation in [37], in which the position of the vehicle, the origin of the body frame, is defined as $\mathbf{p}^n = [x, y, z]^T$, the velocity is defined as $\mathbf{v}^n$, and the position of sender i is defined as $\breve{\mathbf{p}}_i^n = [\breve{x}_i, \breve{y}_i, \breve{z}_i]^T$, all in the NED frame. The underwater AWS is modeled as $c = \sqrt{\beta}c_0$, where c_0 is the assumed wave speed. Furthermore, as the base receiver on the vehicle is not assumed to be in the origin of the body frame, we define $\mathbf{r}_{\text{base}}^b$ as the known vector from the origin of the body frame to the base receiver, given in the body frame. The geometric range is defined as $\rho_i = ct_i = ||\mathbf{p}^n + \mathbf{R}_b^n(\mathbf{\Theta})\mathbf{r}_{\text{base}}^b - \breve{\mathbf{p}}_i^n|| = ||\mathbf{p}_{br}^n - \breve{\mathbf{p}}_i^n||$ where $\mathbf{p}_{br}^n$ is the position of the base receiver in the NED frame, c is the wave speed, t_i is the TOA from sender i, and $||\cdot||$ is the 2-norm. Consequently, the range measurements are modeled as

$$y_i = \frac{1}{\sqrt{\beta}}(\rho_i + \epsilon_{y,i}), \qquad i = 1, \ldots, N \qquad (3)$$

where $\epsilon_{y,i}$ is the zero-mean Gaussian white noise with variance $\sigma_{y,i}^2$ and $\beta > 0$ is an unknown multiplicative parameter to take into account uncertainty in the underwater AWS.

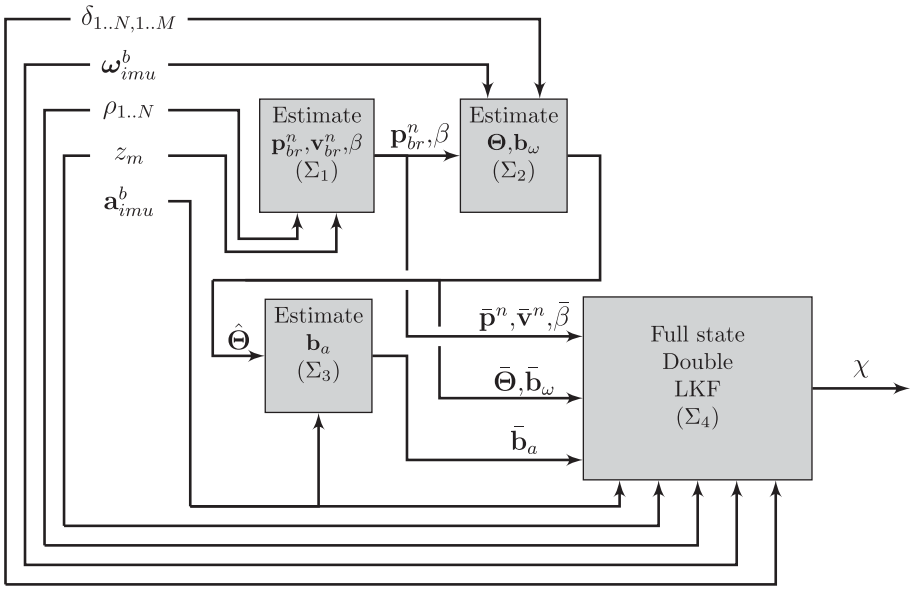

Fig. 2. Observer structure. Measurements enter through each block on either the top or the bottom, inputs from other blocks enter on the left side, marked with how the input is used, and outputs come out on the right side.

The DTOA measurements are found on subtracting pseudoranges, based on the formulation in [1]. Each pseudorange difference $\delta_{i,j}$ is modeled as

$$\delta_{i,j} = \frac{1}{\sqrt{\beta}} \left(||\mathbf{p}^n + \mathbf{R}^n_b \mathbf{d}^b_j - \breve{\mathbf{p}}_i{}^n|| - \rho_i + \epsilon_{\delta,i,j} \right), \quad i = 1, \ldots, N, \quad j = 1, \ldots, M \tag{4}$$

where $\epsilon_{\delta,i,j}$ is the zero-mean Gaussian white noise with variance $\sigma^2_{\delta,i,j}$ and $\mathbf{d}^b_j$ is the vector j between receivers, expressed in the body frame. Furthermore, depth measurements are also employed, modeled as

$$z_m = z + \epsilon_z \tag{5}$$

where ϵ_z is assumed to be zero-mean Gaussian white noise with variance σ^2_z.

Assumption 1: At least two of the vectors between receivers $\mathbf{d}^n_j$ are nonparallel for all t, i.e.,

$$\exists\, c \quad \text{s.t.} \sum_{i \in \{1,\ldots,M\}} \sum_{j \in \{1,\ldots,M\} \setminus \{i\}} ||\mathbf{d}^n_i \times \mathbf{d}^n_j|| \geq c > 0 \quad \forall\, t.$$

Intuitively, this makes sense, as determining attitude requires at least two nonparallel vectors [17], and parts of the suggested observer are based on determining attitude solely by using TDOA measurements.

Assumption 2: The *N* senders are not collinear.

This assumption is related to the determination of both position and attitude. For position estimation, the assumption can be understood practically by considering three senders in the two-dimensional (2-D) case (which is relevant because of the depth measurement). If the three senders are collinear, it will be impossible to decide based on ranges alone on which side of the line through all three senders the vehicle actually is, because the distance to the line and thus the senders will be the same on each side. Consequently, to determine position unambiguously with only ranges and a depth measurement, the senders cannot be collinear.

Assumption 3: The position of a sender and a receiver is never identical or estimated to be identical.

This is more of a theoretical assumption with regard to stability, as this is impossible in a real scenario. However, if the geometric range between a sender and a receiver is 0, the Jacobian of the pseudorange and pseudorange difference measurements will be singular.

III. PVA, AWS, Rate Sensor Bias, and Accelerometer Bias Observer

As mentioned in Section I-A, the suggested observer is based on the XKF principle, in which an auxiliary estimator is used to provide a linearization point for an LKF, which simplifies proving stability significantly. The overall structure of the proposed observer is shown in Fig. 2. As can be seen from Fig. 2, there are no feedback loops, and the output of the observer is the output of Σ_4. Consequently, the resulting stability analysis is a question of the model in the LKF in Σ_4 being uniformly completely observable (UCO) and uniformly completely controllable (UCC), given that the linearization point provided has proven stability [31]. This is in contrast to the EKF, in which the stability has not been proven for the suggested model, and is far more complicated to analyze, as there is a feedback loop due to the linearization about the LKFs own state estimate. In Sections III-A– III-D, each subsystem will be shortly presented, and the theoretical results will be summarized. The subsystems are described in more detail in the appendices. We define

$$\tilde{\mathbf{x}} := \hat{\mathbf{x}} - \mathbf{x} \tag{6}$$

where $\mathbf{x}$ is a state, as the error between the real state and the estimated state.

Lemma 1: Consider the linear system given by

$$\begin{aligned} \dot{x}(t) &= \mathbf{F}(t)x(t) \\ y(t) &= \mathbf{H}(z,t)x(t) \end{aligned} \tag{7}$$

where z is a state estimated from an external observer in which the error dynamics is GES. The estimate from this observer is denoted by $\check{z}$. Assume the pair $(\mathbf{F}(t), \mathbf{H}(\check{z},t))$ is UCO. Furthermore, assume $x(t)$ is bounded and $||\mathbf{H}(z,t) - \mathbf{H}(\check{z},t)|| \leq k_d||\tilde{z}||^2$ for some $k_d > 0$.

Then, the origin $\tilde{x} = 0$ of the error dynamics of a KF using $\check{z}$ instead of z in the model in (7) is GES.

Proof: See Appendix B. ■

A. Subsystem Σ_1: Estimate $\mathbf{p}^n_{br}$, $\mathbf{v}^n_{br}$, β.

Subsystem Σ_1 consists of an algebraic transform followed by a linear KF for estimating position, velocity, and AWS using pseudorange and depth measurements, and is based on the approach suggested in [29]. For more details regarding Σ_1, see Appendix A-A.

Lemma 2: Point $(\tilde{\mathbf{p}}^n_{br}, \tilde{\mathbf{v}}^n_{br}, \tilde{\beta}) = (\mathbf{0}, \mathbf{0}, 0)$ of the error dynamics of the system Σ_1 is GES under Assumptions 2 and 3.

Proof: See [29]. Two extra assumptions are formulated in [29] for the system to be GES, in which one regards an optional addition to the estimator to increase accuracy in some cases, and the other is fairly trivial to achieve in practice. Therefore, for simplicity, these have not been included in this article. However, they are also necessary assumptions for Σ_1 to be stable. ■

B. Subsystem Σ_2: Estimate $\mathbf{\Theta}$, $\mathbf{b}_\omega$

Subsystem Σ_2 is an observer based on the XKF principle, suggested in [2], estimating attitude and rate sensor bias, based on an estimate of $\mathbf{p}^n$ and β, and pseudorange difference and rate sensor measurements. For more details regarding Σ_2, see Appendix A-B.

Lemma 3: Point $(\tilde{\mathbf{p}}^n_{br}, \tilde{\mathbf{v}}^n_{br}, \tilde{\beta}, \tilde{\mathbf{\Theta}}, \tilde{\mathbf{b}}_\omega) = (\mathbf{0}, \mathbf{0}, 0, \mathbf{0}, \mathbf{0})$ of the error dynamics of the cascaded system $\Sigma_1 - \Sigma_2$ is exponentially stable under Assumptions 1–3.

Proof: See [2] for proof of the nominal system, combined with Lemma 1 in which Assumption 3 ensures that $||\mathbf{H}(z,t) - \mathbf{H}(\check{z},t)|| \leq k_d||\tilde{z}||^2$ where z is the output from Σ_1. Unfortunately, it is impossible to obtain global stability properties due to the singularities $\theta = \pi/2 + k\pi,\ k \in \mathbb{Z}$. ■

C. Subsystem Σ_3: Estimate $\mathbf{b}_a$

Subsystem Σ_3 is a linear KF estimating $\mathbf{b}_a$ based on accelerometer measurements and taking attitude from Σ_2 as a time-varying input. The system model is given by

$$\Sigma_3 : \begin{aligned} \dot{\mathbf{b}}_a &= \epsilon_{ba} \\ \mathbf{y}_b &= \mathbf{b}_a + \epsilon_{yb} \end{aligned} \tag{8}$$

where ϵ_{ba} and ϵ_{yb} are vectors with zero-mean Gaussian white noise with covariance $\mathbf{Q}_{ba}$ and $\mathbf{R}_{yb}$, respectively. Similar to Σ_1, in Σ_3, the acceleration of the vehicle is assumed to be unknown and is modeled as white noise. For more details regarding Σ_3, see Appendix A-C.

Lemma 4: Point $(\tilde{\mathbf{\Theta}}, \tilde{\mathbf{b}}_\omega, \tilde{\mathbf{b}}_a) = (\mathbf{0}, \mathbf{0}, \mathbf{0})$ of the error dynamics of the cascaded system $\Sigma_2 - \Sigma_3$ is exponentially stable under Assumptions 1–3.

Proof: It is straightforward to show that the model in Σ_3 is uniformly observable and controllable, thus the error dynamics of a linear KF based on the model are GES. As $\mathbf{y}_b$ is generated from a constant vector multiplied with a rotation matrix (see Appendix A-C), leaving $\mathbf{H}$ bounded, it follows from Lemma 1 that the cascade is LES with singularities $\theta = \pi/2 + k\pi$, $k \in \mathbb{Z}$. ■

D. Subsystem Σ_4: Full-State Double LKF

Subsystem Σ_4 is a double LKF using the output from $\Sigma_1 - \Sigma_3$ as linearization point. The observer estimates PVA, AWS, rate sensor bias, and accelerometer bias using pseudorange, pseudorange difference, accelerometer, rate sensor, and depth measurements. The system model is given by

$$\dot{\chi} = \begin{bmatrix} \mathbf{v}^n \\ \mathbf{R}^n_b(\mathbf{\Theta})(\mathbf{a}^b_{\text{imu}} - \mathbf{b}_a - \epsilon_a) + \mathbf{g}^n \\ \epsilon_\beta \\ \epsilon_{b_a} \\ \mathbf{T}(\mathbf{\Theta})(\boldsymbol{\omega}^b_{\text{imu}} - \mathbf{b}_\omega - \epsilon_\omega) \\ \epsilon_{b_\omega} \end{bmatrix}$$

$$\Sigma_4 : \quad \mathbf{y} = \begin{bmatrix} \rho_1 \\ \vdots \\ \rho_N \\ \delta_{1,1} \\ \vdots \\ \delta_{N,M} \\ z \\ -\mathbf{R}^b_n(\mathbf{\Theta})\mathbf{g}^n + \mathbf{b}_a \end{bmatrix} + \begin{bmatrix} \epsilon_{y,1} \\ \vdots \\ \epsilon_{y,N} \\ \epsilon_{\delta,1,1} \\ \vdots \\ \epsilon_{\delta,N,M} \\ \epsilon_z \\ \epsilon_\alpha \end{bmatrix} \tag{9}$$

where $\chi = [\mathbf{p}^{n\,T}, \mathbf{v}^{n\,T}, \beta, \mathbf{b}_a^T, \mathbf{\Theta}^T, \mathbf{b}_\omega^T]^T$, $\mathbf{R}^n_b$ is defined in Section II-B, and $\mathbf{T}(\mathbf{\Theta})$ is derived in [35], given by

$$\mathbf{T} = \begin{bmatrix} 1 & \text{s}\phi\text{t}\theta & \text{c}\phi\text{t}\theta \\ 0 & \text{c}\phi & -\text{s}\phi \\ 0 & \text{s}\phi/\text{c}\theta & \text{c}\phi/\text{c}\theta \end{bmatrix} \tag{10}$$

where $\text{s}\cdot := \sin(\cdot)$, $\text{c}\cdot := \cos(\cdot)$, and $\text{t}\cdot = \tan(\cdot)$; ϵ_β is zero-mean Gaussian white noise with variance σ^2_β; ϵ_a, ϵ_{b_a}, ϵ_ω, ϵ_{b_ω}, and ϵ_α are vectors with zero-mean Gaussian white noise with covariances $\mathbf{Q}_a$, $\mathbf{Q}_{b_a}$, $\mathbf{Q}_\omega$, $\mathbf{Q}_{b_\omega}$, and $\mathbf{Q}_\alpha$, respectively; ρ_i is given in (3); $\delta_{i,j}$ is given in (4); and $\epsilon_{y,i}$, $\epsilon_{\delta,i,j}$, and ϵ_z are zero-mean Gaussian white noise, with variances $\sigma^2_{y,i}$, $\sigma^2_{\delta,i,j}$, and σ^2_z, respectively. For more details regarding Σ_4, see Appendix A-D.

Lemma 5: The nominal system Σ_4 is UCO and UCC.

Proof: See Appendix C. ■

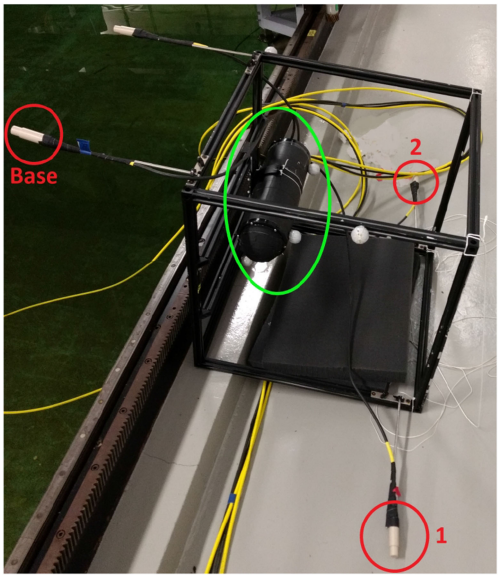

Fig. 3. Aluminum frame with receiver setup. In the image, the frame is tilted sideways. Base receiver, receiver 1, and receiver 2 are marked with red circles. The tube containing the IMU is within the green ellipse.

Theorem 1: Point $(\tilde{\mathbf{p}}^n_{br}, \tilde{\mathbf{v}}^n_{br}, \tilde{\beta}, \tilde{\mathbf{\Theta}}, \tilde{\mathbf{b}}_\omega, \tilde{\mathbf{b}}_a, \tilde{\chi}) = (\mathbf{0}, \mathbf{0}, 0, \mathbf{0}, \mathbf{0}, \mathbf{0}, \mathbf{0})$ of the error dynamics of the cascaded system $\Sigma_1 - \Sigma_4$ is exponentially stable under Assumptions 1–3.

Proof: The observers providing the linearization points have been shown to be either GES (Σ_1) or LES with singularities $\theta = \pi/2 + k\pi,\ k \in \mathbb{Z}$ (Σ_2 and $\Sigma_2 - \Sigma_3$). As stated in [31], if the given model in Σ_4 is UCO and UCC, the error dynamics of the cascade consisting of the LKF in Σ_4 using the outputs from $\Sigma_1 - \Sigma_3$ as linearization points will inherit the stability properties of the estimators generating the linearization point (in this case, LES with singularities $\theta = \pi/2 + k\pi,\ k \in \mathbb{Z}$). ■

IV. System Setup, Calibration, and Implementation Aspects

A. System Setup

For ground truth measurements, a Qualisys underwater camera positioning system with measurement frequency of approximately 50 Hz is employed, giving six-degrees-of-freedom measurements of the ROV, with stated millimeter precision for position and subdegree precision on the attitude. However, this is under optimal circumstances, and during testing, some inaccuracies in attitude occurred. Consequently, only position and heading were used as ground truth from the Qualisys system, and the rest of the states were estimated by using an EKF with the ground truth as input.

The vehicle for which the state is estimated is an aluminum frame, made for testing of underwater estimation algorithms. A tube containing the IMU and electronics is attached to the frame, along with acoustic receivers and markers for the camera positioning system (see Fig. 3 for an image).

The IMU used is an ADIS16485, a microelectromechanical IMU with a price of around $1600, with specifications shown in Table I. The IMU data is read with a frequency of 100 Hz.

TABLE I
IMU Specification

In-run Gyro Rate Bias Stability	$6.25\,\mathrm{deg/h}$
Angular Random Walk	$0.3\,\mathrm{deg}/\sqrt{\mathrm{h}}$
In-run Accelerometer Bias Stability	$0.032\,\mathrm{mg}$
Velocity Random Walk	$0.023\,\mathrm{m/s/h}$

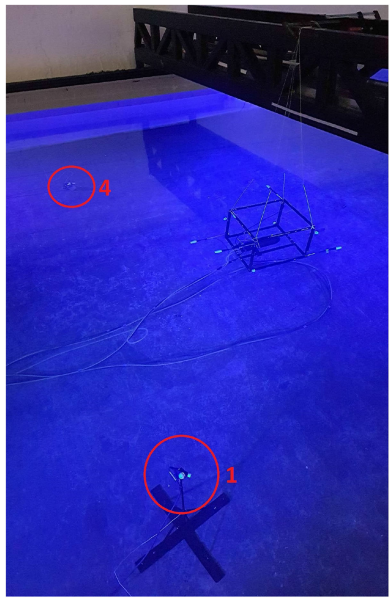

Fig. 4. Test vehicle and sender setup. Two senders are visible and marked with red circles.

The acoustic system used is a development kit provided by Waterlinked [38], consisting of four senders and three receivers. An image of the aluminum frame along with two of the senders is shown in Fig. 4. Waterlinked specializes in short-range accurate positioning for underwater vehicles. A ranging algorithm has been developed for use on the development kit. The intended use of the acoustic system is in parts of inspection, maintenance, and repair operations in which there is a demand for high-accuracy state estimation, within a small area of up to 100 m × 100 m. Two senders were placed on the sea bottom at about 1.5 m depth, and two senders were placed around 0.7 m above the sea bottom. Three receivers were attached to the aluminum frame, as this is the minimum amount of receivers necessary. Adding more receivers might increase accuracy, but it is also important to show performance for the minimum amount of receivers required, with regard to system complexity.

B. Calibration

As there are several system parameters that must be known accurately, especially with regard to the acoustic system, calibration is needed.

For a description of possible IMU error sources, see [39]. However, as the IMU used is rather expensive, and of high quality, and the body coordinate system is defined as the IMU

TABLE II
CALIBRATION RESULTS

Parameter	$\breve{\mathbf{p}}_1^n$	$\breve{\mathbf{p}}_2^n$	$\breve{\mathbf{p}}_3^n$	$\breve{\mathbf{p}}_4^n$
x[m]	-0.469	4.74	4.33	-0.429
y[m]	1.92	1.13	-2.01	-2.09
z[m]	-0.697	-0.169	-0.701	-0.116
Parameter	$\mathbf{r}_{base}^b$	$\mathbf{d}_1^b$	$\mathbf{d}_2^b$	
x[m]	0.302	0.399	-0.819	
y[m]	0.317	-0.573	-0.576	
z[m]	0.428	-0.796	-0.774	

coordinate system, no calibration seemed necessary, except for estimating the magnitude of the gravity acceleration. As the heading angle was found from the Qualisys system, the possibility of a rotational offset in yaw angle between the Qualisys body coordinate system and the IMU coordinate system was apparent. However, actions were taken to minimize this offset when choosing the Qualisys body coordinate system, such that no calibration seemed necessary.

For calibrating sender and receiver positions, a nonlinear optimization scheme was run, minimizing the difference between the measured pseudorange differences and the geometric range differences calculated from the Qualisys system and the difference between the measured pseudoranges and the geometric ranges calculated from the Qualisys system with sender and receiver positions as variables, along with the underwater wave speed.

The results from the calibration can be seen in Table II.

C. Implementation Aspects

As mentioned above, the IMU measurement frequency was 100 Hz. This frequency was chosen to be sufficiently high to capture the dynamics of the system while not causing too large of a computational burden. First-order Euler discretization was chosen for all estimators, as the observers using IMU data are run with the same frequency as the IMU. The high frequency compared to the dynamics of the system results in a first-order discretization scheme being sufficient. The linearization scheme chosen for the NLOs is the first-order Taylor series approximation given by

$$\mathbf{f}(\mathbf{v}) \approx \mathbf{f}(\bar{\mathbf{v}}) + \left.\frac{\mathrm{d}\mathbf{f}(\mathbf{v})}{\mathrm{d}\mathbf{v}}\right|_{\mathbf{v}=\bar{\mathbf{v}}} (\mathbf{v} - \bar{\mathbf{v}}) \tag{11}$$

where $\mathbf{f}$ is a vector function, $\mathbf{v}$ is a vector, and $\bar{\mathbf{v}}$ is the linearization point. For a discussion regarding implementation aspects of NLOs, see [40].

1) Pseudorange Measurement Timing Issues: As discussed in [29], at least three pseudorange measurements are needed to perform the algebraic transform in Σ_1 (four if no depth measurement is available). Furthermore, at least three pseudorange difference measurements are needed to perform the algebraic transform in Σ_2. In the experiment, the distances between senders and receivers were small, with a maximum of 5 m. As the senders are synchronized and send at the same time, the offset between received signals is negligible. However, for larger differences in distance between senders and receivers, each acoustic signal might arrive at significantly different times. Even though, as mentioned above, the Waterlinked system is designed for accurate state estimation within a small area of up to 100 m $\times$ 100 m, with a maximum difference in received signal of around 0.1 s, it might still be valuable to discuss handling these differences for general scenarios.

The simplest way of handling acoustic signal offset when performing the algebraic transformations in Σ_1 and Σ_2 is to simply wait until enough measurements have been received. Naturally, an offset in measurements will decrease accuracy, depending on how fast the dynamic of the system is, as the measurements are assumed to be simultaneous, and delayed measurements will give inaccurate information. However, it is important to note that simulations done in [1], [29], and [31] indicate that in general for the XKF, the linearization point provided by the auxiliary estimator can be somewhat inaccurate, depending on system configuration and noise magnitude, and the output of the observer will still be close-to-optimal w.r.t. noise.

A more extensive approach might be to take vehicle position into account, after the position estimator has converged. As the position of the senders on the sea bottom is assumed to be known, an upper bound for transmission time can be set. The accuracy of this scheme depends on many factors; pseudorange measurement noise, distance to senders, probability of lost measurements, and vehicle velocity.

Receiving acoustic signals from each sender at different times is not a problem for the subsystems of Σ_1 and Σ_2 containing an LKF and Σ_4, as the measurement equations are based on each separate acoustic signal, and can consequently be modified based on which signal has been received. Offset in acoustic measurements is not a problem for Σ_3 either, as it only uses IMU measurements and the input from Σ_2.

Each acoustic wave needs to be received, registered, and processed to be used as a pseudorange measurement. This results in a natural time delay for each measurement. As the data in this case have been postprocessed, the UNIX timestamp for each measurement has been used as the timestamp, but in a real-time system, ways of handling this delay must be applied; see, for example, [27] and [41].

2) Handling Outliers: Σ_1 is suitable for performing outlier detection. Outliers occurred during testing, and a common outlier detection scheme based on the Mahalanobis distance seemed sufficient. The Mahalanobis distance is given by [42]

$$d_{Ma} = \nu_k^T \mathbf{S}^{-1} \nu_k \tag{12}$$

where $\nu_k = y_i - \hat{y}_i$ and $\mathbf{S} = \mathbf{H}_{k,i}\mathbf{P}_{k+1/k}\mathbf{H}_{k,i}^T + \sigma_{y,i}^2$ is the filter innovation covariance. $\mathbf{H}_{k,i}$ is the Jacobian of (3) for measurement i. d_{Ma} is calculated for each pseudorange measurement, and a measurement is rejected if d_{Ma} is above a given threshold, i.e., γ_{Ma}.

As it is necessary to perform outlier detection for all receivers, $M+1$ instances of Σ_1 are run, one related to each receiver.

TABLE III
PERCENTAGE OF TOTAL COMPUTATIONAL LOAD FOR EACH SUBSYSTEM

Subsystem	Σ_1	Σ_2	Σ_3	Σ_4
Load percentage	9.0 %	40.9 %	0.5 %	49.6 %

For the base receiver, the estimated position, velocity, and β is used in the observer, whereas for the M other receivers, the observer is used solely for outlier detection. As mentioned above, the observer is updated with the same frequency as the pseudorange measurements, typically 1 Hz, but less computationally demanding outlier detection schemes can be constructed if necessary.

Handling outliers is similar to handling delayed and lost measurements. If the minimum number of measurements necessary for the algebraic transformations in Σ_1 and Σ_2 to be possible is not accepted, the updates in these subsystems are simply skipped at the given time, and the system starts waiting for new measurements.

For other approaches regarding outlier robust underwater estimation schemes, see, for example, [43]–[45].

3) Computational Load: In general, observers that employ IMU measurements are run at the same frequency as the IMU, whereas observers that only employ pseudorange or pseudorange difference measurements are run at the same frequency as these measurements.

Consequently, Σ_1 is run with a frequency of 1 Hz, whereas Σ_2 and Σ_4 are run with a frequency of 100 Hz. It seemed sufficient to run Σ_3 with a frequency of 1 Hz, although this can be increased if necessary.

Σ_2 and Σ_4 are both designed as complimentary filters; applying IMU measurements as input to the system instead of in the measurement model. Consequently, the steps with the main computational load is when pseudorange and pseudorange difference measurements are available. For the given scenario, this is at 1 Hz, in which more complex operations are needed, especially matrix inversions.

From this analysis, it seems that the main computational load is in Σ_2 and Σ_4. It is of value to compare the computational complexity to an EKF for the same model, as this can be seen as a natural alternative to the suggested observer (although this would require sacrificing proven stability properties). The percentage of total computational load for each subsystem is shown in Table III. As the EKF is a single LKF using its own state as linearization point, an EKF based on the same system model as in Σ_4 will have half the computational load as Σ_4. Consequently, the computational load for the suggested observer was around four times that of the EKF in MATLAB for the given setup and measurement frequencies (this is a rough estimate as this relationship is very dependent on implementation).

V. TESTING AND RESULTS

In the experiment, the vehicle is fairly stationary in position, within a rather small volume of around 0.5 m $\times$ 0.5 m $\times$ 0.5 m. The reason for this is that the vehicle is required to stay within a high-accuracy and reliable coverage area of the Qualisys positioning system. First, the vehicle is kept stationary, in which the roll angle is increased and decreased, then the pitch angle is increased and decreased. The experiment ends with a more chaotic maneuver in which roll, pitch, yaw angle, and position are varied. Ground truth position and attitude can be seen in Fig. 5.

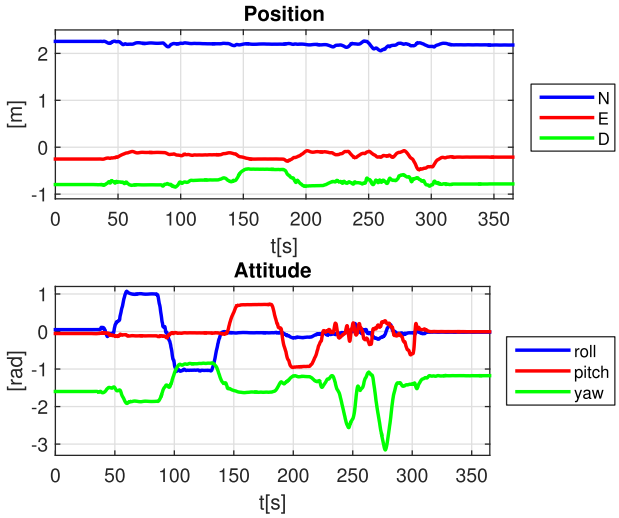

Fig. 5. Ground truth position and Euler angles from the Qualisys system.

As mentioned in Section IV-A, the Qualisys system has very accurate position and attitude measurements during optimal circumstances. However, optimal circumstances are usually not the case, due to varying lighting conditions, camera properties, and other factors. As the gravity vector is dominating the accelerometer measurement, inaccurate roll and pitch output from the Qualisys system can have significant effects on the acceleration measurement rotated to the NED frame. However, position and heading measurements do not have such high accuracy requirements. Consequently, position and heading from the Qualisys system were used as very accurate measurements along with accelerometer measurements in an EKF estimating position, velocity, acceleration, accelerometer bias, attitude, rate sensor bias, and gravity. The output from this EKF is used as ground truth.

As the sensors used did not include a pressure sensor, the depth measurements are simulated, based on the ground truth position with added Gaussian noise with a realistic magnitude. In the authors' opinion, this does not compromise the results, as a pressure sensor is very cheap and accurate and has a high measurement frequency (in the experiment, the simulated depth measurements had a frequency of 1 Hz).

To show both transient and stationary performances, all subsystems were initialized with inaccurate initial vales. As the suggested observer has proven stability, it will converge for all initial conditions that does not cause it to encounter one of the singularities. The tuning parameter values for each subsystem were chosen through a mix of trial and error, considering stability requirements for the NLO, considering the maximum expected rate of change for the system, and for measurement covariance matrices, the noise was assumed independent and the variance was found by looking at the measurement noise when

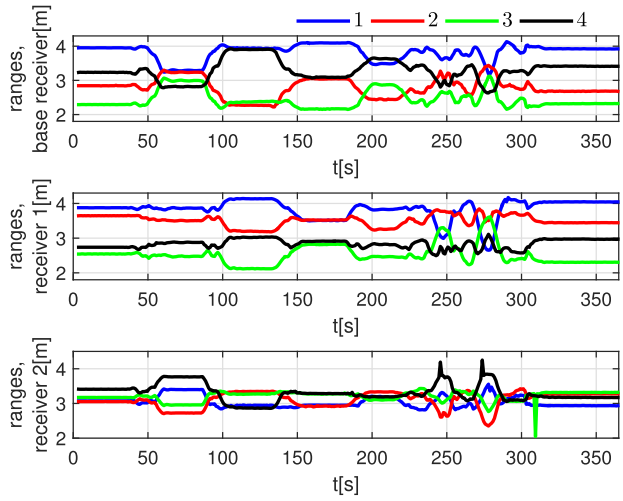

Fig. 6. Raw measured pseudoranges for all three receivers. Pseudorange i is the range measured from the sender at $\check{\mathbf{p}}_i^n$.

the vehicle was stationary. The tuning parameter values for each subsystem can be seen in Table IV. $\mathbf{P}_0$ is the initial covariance matrix for the KFs, $\mathbf{x}_0$ is the initial estimate for each subsystem, and $\mathbf{k}_{i\,x\,j}$ means an i times j matrix containing the value $\mathbf{k}$. $\mathrm{diag}(\mathbf{v})$ is a diagonal matrix with the vector $\mathbf{v}$ along the diagonal.

As the claim is that the observer has close-to-optimal noise performance, along with the mathematically proven stability, it is of value to compare to an EKF, as the EKF is assumed to also have close-to-optimal noise performance and is a relevant alternative to the suggested observer. The EKF is run with the same model and tuning as Σ_4, except that the linearization point used is the observer's own state. The output from the EKF is denoted by χ_{EKF}. Furthermore, it would be useful to also have an impression of the optimal performance. An LKF linearized around the true state would give very close-to-optimal performance, as this would in principle be a linear Kalman filter for each time step (if higher order terms of the linearization are neglected, which seems to be a valid assumption in this case). Consequently, the LKF in Σ_4 is also run, using the ground truth as linearization point. This filter is also tuned in the same way as the LKF in Σ_4, and the output of this filter is denoted by χ_{opt}.

A. Results

The raw pseudorange measurements can be seen in Fig. 6, and it can be seen that the first measurement occurs at $t \approx 2.8$ s. Throughout the experiment, around 0.2% of the pseudorange measurements were rejected as outliers. It is worth noting that the pool in which the experiment was conducted is narrow and shallow, about 40 m $\times$ 6.45 m $\times$ 1.5 m, suggesting that the acoustic ranging scheme developed is robust w.r.t. echo and multipath. The linearization point used in Σ_4 consisting of state estimates from Σ_1, Σ_2, and Σ_3 is denoted as $\bar{\chi}$. The estimated and real values of $\mathbf{d}_{1,2}^n$ are shown in Fig. 7, the estimated position errors are shown in Fig. 8, and the Euler angle errors are shown in Fig. 9. As there is no ground truth for rate sensor bias and accelerometer bias, the estimates are

TABLE IV
TUNING PARAMETER VALUES

Parameter	σ_β^2	$\mathbf{Q}_a$	$\sigma_{y,i}^2$	σ_z^2
Value	$(1 \cdot 10^{-3})^2$	$0.5^2 \cdot \mathbf{I}_3$	0.02^2	0.05^2

Parameter	γ_{Ma}	$\mathbf{x}_0$	$\mathbf{P}_0$
Value	3	$\begin{bmatrix} \mathbf{0}_{3x1} \\ 1 \\ \mathbf{0}_{3x1} \end{bmatrix}$	$\mathrm{diag}(\begin{bmatrix} \mathbf{5}_{3x1}^2 \\ \mathbf{0.1}_{4x1}^2 \end{bmatrix})$

(a) Values for Σ_1

Parameter	$\mathbf{Q}_d$	$\sigma_{\delta,i,j}^2$
Value	$3^2 \cdot \mathbf{I}_3$	0.2^2

Parameter	$\mathbf{x}_0$	$\mathbf{P}_0$
Value	$\mathbf{0}_{6x1}$	$\mathrm{diag}(\mathbf{0.5}_{6x1}^2)$

(b) Values for $\Sigma_{2,1}$

Parameter	k_I	K_p	σ
Value	0.025	$5 \cdot \mathbf{I}_3$	1

Parameter	M_b	$M_{\hat{b}}$	$\mathbf{x}_0$
Value	0.39	0.4	$[1, 1, 0, \mathbf{0}_{1x3}]^T$

(c) Values for $\Sigma_{2,2}$

Parameter	$\mathbf{Q}_\omega$	$\mathbf{Q}_b$	$\mathbf{R}_a$
Value	$0.05^2 \cdot \mathbf{I}_3$	$\left(1 \cdot 10^{-4}\right)^2 \cdot \mathbf{I}_3$	$\mathrm{diag}([\mathbf{0.2}_{8x1}^2])$

Parameter	$\mathbf{x}_0$	$\mathbf{P}_0$
Value	$[1, 1, 0, \mathbf{0}_{1x3}]^T$	$\mathrm{diag}(\begin{bmatrix} \mathbf{2}_{3x1}^2 \\ \mathbf{0.1}_{3x1} \end{bmatrix})$

(d) Values for $\Sigma_{2,3}$

Parameter	$\mathbf{Q}_{ba}$	$\mathbf{Q}_a$
Value	$\left(1 \cdot 10^{-3}\right)^2 \cdot \mathbf{I}_3$	$0.1^2 \cdot \mathbf{I}_3$

Parameter	$\mathbf{x}_0$	$\mathbf{P}_0$
Value	$\mathbf{0}_{3x1}$	$0.1^2 \cdot \mathbf{I}_3$

(e) Values for Σ_3

Parameter	$\mathbf{Q}_a$	σ_β^2	$\mathbf{Q}_{b_a}$
Value	$0.1^2 \cdot \mathbf{I}_3$	$(1 \cdot 10^{-4})^2$	$(1 \cdot 10^{-4})^2 \cdot \mathbf{I}_3$

Parameter	$\mathbf{Q}_\omega$	$\mathbf{Q}_{b_\omega}$	$\sigma_{y,i}^2$
Value	$0.05^2 \cdot \mathbf{I}_3$	$(1 \cdot 10^{-4})^2 \cdot \mathbf{I}_3$	0.05^2

Parameter	$\sigma_{\delta,i,j}^2$	σ_z^2	$\mathbf{R}_\alpha$
Value	0.2^2	0.05^2	$0.3^2 \cdot \mathbf{I}_3$

Parameter	$\mathbf{Q}_\alpha$	$\mathbf{x}_0$	$\mathbf{P}_0$
Value	$0.3^2 \cdot \mathbf{I}_3$	$[\mathbf{0}_{1x6}, 1, \mathbf{0}_{1x3}, 1, 1, 0, \mathbf{0}_{1x3}]^T$	$\mathrm{diag}(\begin{bmatrix} \mathbf{5}_{3x1}^2 \\ \mathbf{1}_{3x1} \\ \mathbf{0.1}_{4x1}^2 \\ \mathbf{2}_{3x1}^2 \\ \mathbf{0.1}_{3x1}^2 \end{bmatrix})$

(f) Values for Σ_4

Σ_2 consists of several steps (see Appendix A-B for details).

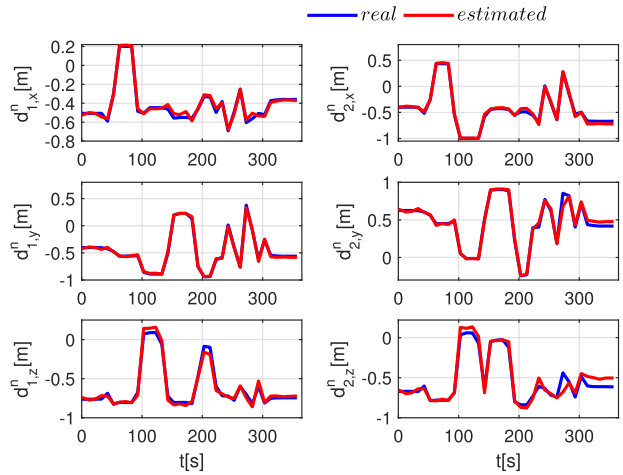

Fig. 7. Real and estimated values for $\mathbf{d}_1^n = [d_{1,x}, d_{1,y}, d_{1,z}]^T$.

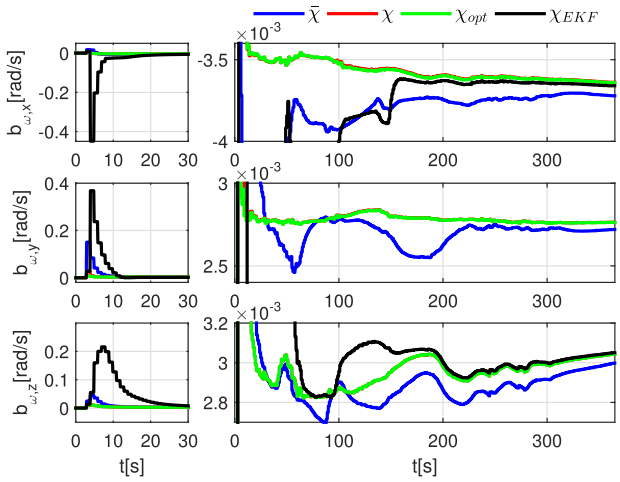

Fig. 10. Estimated rate sensor bias. Two axis are chosen to show both transient and stationary behaviors.

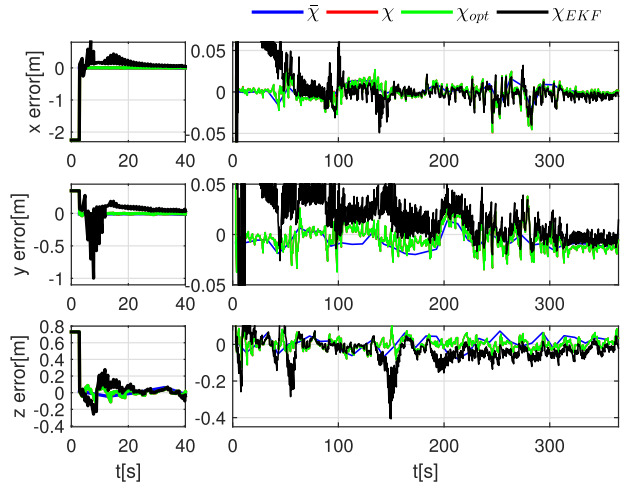

Fig. 8. Position estimation errors. Two axis are chosen to show both transient and stationary behaviors.

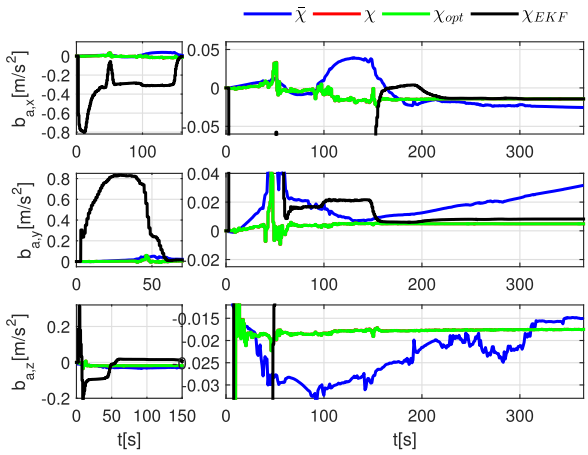

Fig. 11. Estimated accelerometer bias. Two axis are chosen to show both transient and stationary behaviors.

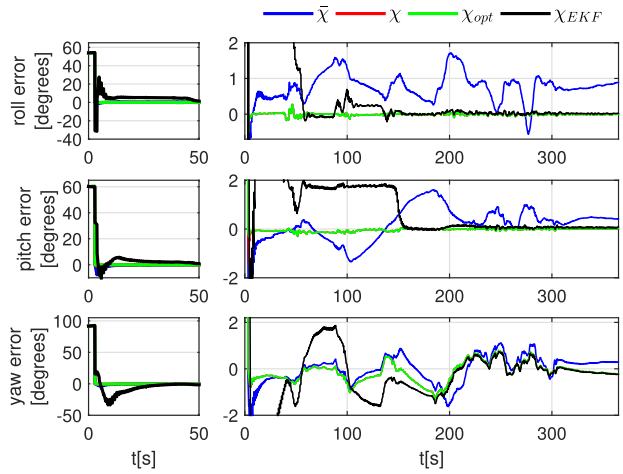

Fig. 9. Euler angle estimation errors. Two axis are chosen to show both transient and stationary behaviors.

shown and not the estimate errors. However, estimates from the EKF generating ground truth mentioned above are available, and are used in the LKF generating χ_{opt}. The calculated biases in calibration are $\mathbf{b}_{a\,\text{cal}} = [-1.4, 0.46, -1.7] \cdot 10^{-2}$ and $\mathbf{b}_{\omega\,\text{cal}} = [-3.7, 2.8, 3.2] \cdot 10^{-3}$, whereas the final estimate for the suggested observer is $\mathbf{b}_{a\,\chi} = [-1.4, 0.49, 1.8] \cdot 10^{-2}$ and $\mathbf{b}_{\omega\,\chi} = [-3.6, 2.8, 3.0] \cdot 10^{-3}$. This is within calibration uncertainty approximated by the standard deviations extracted from the ground truth EKF covariance matrix (around $2.8 \cdot 10^{-3}$ for $\mathbf{b}_{a\,\text{cal}}$ and around $3.4 \cdot 10^{-4}$ for $\mathbf{b}_{\omega\,\text{cal}}$), and similar results considering the magnitude of the measurement noise. Rate sensor bias estimates are shown in Fig. 10, and accelerometer bias estimates are shown in Fig. 11.

It is apparent that the linearization point used in Σ_4, $\bar{\chi}$, is less accurate than the output of Σ_4, as proposed. This fits well with the principle of the XKF, in which the estimators providing the linearization point are designed to have proven stability, and not for close-to-optimal performance w.r.t. noise, whereas the LKF

TABLE V
RMSE AFTER CONVERGENCE FOR ALL ESTIMATION SCHEMES

		$\mathbf{p}^n$	Θ
[States][unit]		$[x, y, z]$[m]	$[\psi, \theta, \phi]$[degrees]
RMSE	$\bar{\chi}$	$[0.0076, 0.012, 0.035]$	$[0.89, 0.71, 0.66]$
	χ	$[0.0095, 0.012, 0.028]$	$[0.028, 0.066, 0.44]$
	χ_{EKF}	$[0.0085, 0.014, 0.053]$	$[0.038, 0.078, 0.54]$
	χ_{opt}	$[0.0096, 0.012, 0.028]$	$[0.028, 0.066, 0.44]$

Time of convergence was chosen as $t = 160$ s for the EKF and $t = 50$ s for the other estimators.

is employed to get close-to-optimal performance w.r.t. noise in addition to the proven stability.

In general, the suggested observer converges, and it performs almost identically to the optimal LKF using the true state as the linearization point. After the EKF has converged, the stationary performance is similar to the suggested observer and the optimal LKF, but the transient period of the EKF is longer and has larger deviations from the true state. The root-mean-squared error (RMSE) after convergence for each estimation scheme can be seen in Table V. It is apparent that the RMSE of the suggested observer is almost identical to the optimal filter. It is also worth noting that the chosen time of convergence is around three times longer for the EKF. As mentioned above, the EKF takes significantly longer time to converge, which can also be seen in the plots.

It is apparent that the RMSE in yaw angle is larger than those for roll and pitch angle, for all estimators except the linearization point. This can be explained by considering that the attitude is estimated only based on the acoustic signals for the linearization point, whereas the LKF in Σ_4 also relates the accelerometer measurement to the attitude, making it possible to estimate roll and pitch much more accurately. This is done on purpose, as mentioned in Section I, to decouple the attitude estimate from the accelerometer measurement making accelerometer bias estimation more efficient. For increasing the accuracy of the yaw angle estimate, other measurements could be added, such as a magnetometer. However, as mentioned in Section I, the magnetometer suffers from certain drawbacks that can result in a time-varying measurement bias.

VI. DISCUSSION

It is important to notice that the term "optimal performance" discussed in this article is with respect to the given scenario; noise magnitudes, sender placement, receiver placement, expected volume of movement, expected dynamic behavior, and many other factors affect the optimal performance of the observer. Larger distances between senders and receivers might increase measurement noise, and thus decrease accuracy for the suggested observer. Furthermore, the placement of senders and receivers affects the geometric properties of the system, more specifically the conditioning of some matrices used for algebraic transformations in Σ_1 and Σ_2. For optimal positioning, the vector from the senders to the base receiver should be as noncollinear as possible. For optimal attitude estimation, the vector between the base receiver and the senders should be as noncoplanar as possible, and the vectors between receivers should be as noncollinear as possible. This can be considered when placing senders and receivers. An undesirable scenario might occur either if the senders are placed very colinearly or if the vehicle has a much larger distance to the senders than the senders have between each other, neither of which are planned to be scenarios in which the system is applied.

As mentioned in Section V, the tuning for the KFs was decided by estimating the noise in the measured signals, and by considering the expected rate of change in the system. However, for the NLO in Σ_2, the tuning parameters are less intuitive, and a trial-and-error approach was taken. Consequently, better performance for Σ_2 might have been achieved by a different tuning of the NLO, but the chosen tuning seemed to give sufficient accuracy.

As described in Appendix A-C, the acceleration in Σ_3 is modeled as white noise. This is less accurate for vehicles with accelerating vehicles, and the validity of this assumption should be investigated further, even though this is not common for underwater vehicles.

The performance of the EKF could also possibly have been improved by choosing different less realistic tuning parameters, as the inaccurate initial linearization point makes performance unpredictable. This can be seen as a drawback of the EKF, and a different less intuitive and realistic tuning might give better performance for the exact given scenario in the experiment, but will cause unpredictable behavior for other scenarios.

The measurements from the IMU could have been filtered before entering the estimator to decrease noise, for example, by a low-pass filter. However, this would cause an undesirable phase offset, which would need to be handled w.r.t. the other measurements. Furthermore, the unfiltered IMU measurements seemed to give sufficient performance, as long as the measurement noise was properly taken care of in the tuning of each KF.

The measurement model for the acceleration does not take the Coriolis effect into account, as this is considered negligible for the given expected velocity and angular rate for the vehicle. However, this term could be added for underwater vehicles that are expected to either have large velocities or turn quickly while having a linear velocity.

As described in [1], it is possible to take the acceleration measurement (assuming no accelerometer bias) into account in Σ_2 also. As the accelerometer measurement bias is assumed to be zero in [1], the roll and pitch angle estimates from using the accelerometer measurements have a bias. However, as this estimate is only used as a linearization point, a bias in the roll and pitch angles is tolerable, as long as it is small (if the accelerometer bias is small). Furthermore, if the accuracy of the attitude estimate using only acoustics is much lower than using a biased accelerometer measurement, the biased, more accurate estimate may be preferable.

As mentioned in Section IV-A, the reference values used as ground truth are generated by using an EKF taking the Qualisys position and heading measurements at 50 Hz and the accelerometer measurements at 100 Hz as input. As long as the system is

modeled correctly and initialized very close to the actual values, these can be assumed to be very accurate state estimates, as all measurements are very accurate, and have a high measurement frequency. Furthermore, the estimates from the EKF seem to be changing within the accuracy stated by the covariance matrix in the KF, and seem to have behavior that corresponds to a system where the most important parts are modeled.

In the stability proof, building on the stability criteria stated in [31], it is assumed that all noise in the system is zero. However, in [31], it is also stated that "for the general case, when $w \neq 0$ and $e \neq 0$, one can show that bounded w and e give bounded estimation errors." (w is process disturbance and e is the measurement error). In general, the estimates might be suboptimal because the linearization point is correlated with the measurements, as it is also generated from filtering the measurements. Due to the complexity of the system, it is hard to analyze the effect of noise theoretically. Therefore, the sensitivity of the noise for each sensor, along with an analysis regarding how an increasingly inaccurate linearization point affects the system, could be investigated in a detail through Monte Carlo approach. This is considered the further work, although Monte Carlo simulations have been done for Σ_1 in [29] and Σ_2 in [1].

VII. Conclusion

An observer estimating position, velocity, wave speed, accelerometer bias, attitude and rate sensor bias using IMU, depth, pseudorange, and pseudorange difference measurements has been suggested. The observer is based on the XKF principle, in which estimators with proven stability provide a linearization point for an LKF, to achieve an observer for a nonlinear system that has both proven stability and close-to-optimal noise properties w.r.t. zero-mean bounded noise. In contrast to the EKF, which does not have proven stability for the given system, the suggested observer is proven to be LES with singularities $\theta = \pi/2 + k\pi,\ k \in \mathbb{Z}$, which are not likely to occur for most of the conventional underwater vehicles.

Experimental validation is provided, and the observer is compared to an EKF and an optimal nonimplementable filter using the ground truth state as linearization point. The suggested observer converges and stays close to the ground truth values throughout the experiment after convergence. Furthermore, the EKF takes significantly longer to converge, and the proposed observer performs very similarly to the optimal nonimplementable filter both during and after the transient period.

Appendix A
Observer Details

We define $\mathbf{I}_i$ as an $i \times i$ identity matrix, $\mathbf{0}_i$ as an $i \times i$ matrix of zeros, and $\mathbf{0}_{i\times j}$ as an $i \times j$ matrix of zeros.

A. Subsystem Σ_1: Estimate $\mathbf{p}^n_{br}$, $\mathbf{v}^n_{br}$, β

Σ_1 is based on the observer proposed in [29]. The observer in [29] is also based on the XKF principle and contains three stages. However, both simulation and experiments suggest that only two of these stages are necessary to get close-to-optimal performance for the observer suggested in this article. This will also decrease the computational complexity of Σ_1. Consequently, only the first two stages of the observer suggested in [29] are run: In step one, an algebraic transformation is performed to transform the pseudorange and depth measurements into measurements for $\mathbf{p}^n_{br}$ and β, and in step two, these measurements are used as measurements in a linear KF. The algebraic transformation is possible if Assumption 2 is fulfilled, along with two additional assumptions stated in [29]. If scenarios occur in which the accuracy of Σ_1 becomes too low, for example, from increased measurement noise or different sender geometry, the third stage can be included. Due to computational considerations, Σ_1 is run with the same frequency as the pseudorange measurement frequency, and not the depth measurements, which tend to have a much higher frequency.

The KF is based on the system model

$$\begin{aligned}\dot{\mathbf{p}}^n_{br} &= \mathbf{v}^n_{br}\\ \dot{\beta} &= \varepsilon_\beta\\ \dot{\mathbf{v}}^n_{br} &= \varepsilon_a\end{aligned}$$

or written in the matrix form

$$\dot{\chi}_p = \begin{bmatrix}\mathbf{0}_3 & 0 & \mathbf{I}_3\\ \mathbf{0}_3 & 0 & \mathbf{0}_3\\ \mathbf{0}_3 & 0 & \mathbf{0}_3\end{bmatrix}\chi_p + \begin{bmatrix}0 & \mathbf{0}_3\\ 1 & \mathbf{0}_3\\ 0 & \mathbf{I}_3\end{bmatrix}\begin{bmatrix}\varepsilon_\beta\\ \varepsilon_a\end{bmatrix} \tag{13}$$

with measurement

$$\mathbf{y}_p = \begin{bmatrix}\mathbf{I}_4 & \mathbf{0}_{4x3}\end{bmatrix}\chi_p + \varepsilon_{y_p} \tag{14}$$

where $\mathbf{v}^n$ is the velocities in the NED frame and $\chi_p = [\mathbf{p}^{n\,T}_{br}, \beta, \mathbf{v}^{n\,T}_{br}]^T$ is the full-state vector. ε_β and ε_a are the process noises with variance σ^2_β and covariance matrix $\mathbf{Q}_a$, respectively. The covariance matrix of ε_{y_p} is approximated by the first-order linearization and employing finite differences using the central differences approach and the values of $\sigma^2_{y,i}$ and σ^2_z.

B. Subsystem Σ_2: Attitude XKF

Subsystem Σ_2 is based on the observer suggested in [2]. The observer estimates attitude and rate sensor bias using acoustic and rate sensor measurements, which is designed using the XKF principle, and consists of three stages when a position estimate is available. The first stage estimates the vectors between receivers by first employing an algebraic transformation, then using this as input to a linear KF. The tuning parameters of this stage are denoted by $\Sigma_{2,1}$ in Table IV. The second stage is an NLO suggested in [46] that is proven to be GES under Assumption 1 along with some additional criteria: a known upper bound for the rate sensor bias, a design property regarding the matrices used in the estimator is fulfilled, and one of the tuning parameters is above a lower bound, all of which can be ensured when choosing tuning parameters for the NLO. The tuning parameters for this stage are denoted by $\Sigma_{2,2}$ in Table IV. The third stage is an LKF using the output from the NLO in stage two as a linearization point, taking the full nonlinear system into account. The tuning parameters for the third stage are denoted by $\Sigma_{2,3}$ in Table IV. For more details, see [1] and [2].

C. Subsystem Σ_3: Estimate $\mathbf{b}_a$

As the XKF principle is based on an auxiliary estimator providing a linearization point, an auxiliary estimator for $\mathbf{b}_a$ is also needed. Proven stability is necessary for proving the stability of the full-state LKF in Σ_4. It is important to note that simulations and experiments performed using the XKF principle [2], [29], [32] suggest that the linearization point can be inaccurate and still give close-to-optimal noise performance for the LKF. Therefore, the assumptions made in Σ_3 need not be true always, but accurate enough to get a somewhat accurate estimate of $\mathbf{b}_a$.

An NLO estimating position, velocity, and accelerometer bias is suggested in [35]. This NLO is GES under certain criteria for the chosen gains. However, this NLO assumes that the attitude is known, and potential (time-varying) uncertainties in attitude are not taken into account. Consequently, it is hard to find an optimal choice of gain matrices for general scenarios.

The chosen approach for estimating $\mathbf{b}_a$ to use as a linearization point is to use a linear KF. By looking at (1), it is possible to find a measurement for $\mathbf{b}_a$ through some simplifications. If the acceleration is modeled as Gaussian white noise, it is possible to model the acceleration measurement as

$$\mathbf{a}_{\text{imu}}^b = -\mathbf{R}_n^b \mathbf{g}^n + \mathbf{b}_a + \epsilon_a. \tag{15}$$

Furthermore, if the attitude and gravity vector are known, by using the attitude from Σ_2, $\hat{\boldsymbol{\Theta}}$, as a time-varying external input, a measurement for $\mathbf{b}_a$ can be found as

$$\mathbf{b}_a = \mathbf{a}_{\text{imu}}^b + \mathbf{R}_n^b(\hat{\boldsymbol{\Theta}})\mathbf{g}^n - \epsilon_A.$$

The system model is shown in Section III-C. As mentioned above, the attitude is not known, but estimated, and it is beneficial to include this uncertainty in $\mathbf{R}_{yb}$, as this will lead to more accurate estimates for $\mathbf{b}_a$. The chosen way to include attitude uncertainty is by looking at $\mathbf{y}_b$ as a function of acceleration measurement noise, but also attitude noise. By modeling $\mathbf{b}_a$ as a function of both $\mathbf{a}_{\text{imu}}^b$ and the attitude, it is possible to use the finite difference approach to approximate $\mathbf{R}_{yb}$ if the covariances of $\mathbf{a}_{\text{imu}}^b$ and $\hat{\boldsymbol{\Theta}}$ are known or approximated. This fits well with the KF framework, in which an approximation for the uncertainty of $\hat{\boldsymbol{\Theta}}$ is found directly in the covariance matrix of the attitude estimate in the LKF in Σ_2, and $\mathbf{Q}_a$ can be approximated by looking at the accelerometer measurements. A common problem with the LKF is that it is sometimes overconfident, thus underapproximating the covariance matrix. Consequently, the attitude covariance used for calculating $\mathbf{R}_{yb}$ is chosen to be four times the covariance in Σ_2.

D. Subsystem Σ_4: Full-State Double LKF

Σ_4 takes the full nonlinear system into account. The reason for a double LKF is that simulations and experiments have shown that the LKF taking the less accurate output from Σ_1, Σ_2, and Σ_3 as a linearization point is more accurate, but there are still some small deviations. Consequently, as the accuracy of the LKF will be higher if the linearization point is more accurate, the output from this LKF can be used as a linearization point in a second LKF, whereas not sacrificing stability properties as this subsystem also follows the XKF stability criteria.

The system model can be seen in Section III-D. Note that the last entry in the measurement model is based on the accelerometer measurement, and the same approach as described in Appendix A-C has been chosen, in which the acceleration is assumed to be zero, and this uncertainty results in an increased chosen covariance for the measurement noise, ϵ_α, $\mathbf{R}_\alpha$.

As can be seen in Fig. 2, it is $\mathbf{p}_{br}^n$ and not $\mathbf{p}^n$ that is estimated in Σ_1 and used as input to create a linearization point for Σ_4. As attitude information is available, along with a known $\mathbf{r}_{\text{base}}^b$, it is possible to find $\bar{\mathbf{p}}^n$ using the formula $\bar{\mathbf{p}}^n = \bar{\mathbf{p}}_{br}^n - \mathbf{R}_b^n(\bar{\boldsymbol{\Theta}})\mathbf{r}_{\text{base}}^b$. $\bar{\mathbf{v}}_{br}^n$ is used directly as linearization point for $\mathbf{v}^n$, which is not fully accurate, depending on the magnitude of $\mathbf{r}_{\text{base}}^b$ and the magnitude of the rotation of the vehicle. However, as the linearization point need not be fully accurate, it is considered sufficiently accurate for the given scenario. More sophisticated approaches could be applied, for example, compensating by taking the rate sensor measurement into account if necessary.

Appendix B
Proof of Lemma 1

The proof is similar to the proof in [31]. By defining (time dependence has been omitted for simplicity)

$$\mathbf{H}(\check{z}) := \check{\mathbf{H}} \tag{16}$$

we can write the KF estimate dynamic equation as

$$\dot{\hat{x}} = \mathbf{F}\hat{x} + \mathbf{K}(y - \hat{y}) = \mathbf{F}\hat{x} + \mathbf{K}(\mathbf{H}x - \check{\mathbf{H}}\hat{x}) \tag{17}$$

and the error dynamics as

$$\dot{\tilde{x}} = \mathbf{F}x - (\mathbf{F}\hat{x} + \mathbf{K}(\mathbf{H}x - \check{\mathbf{H}}\hat{x})) = \mathbf{F}\tilde{x} + \mathbf{K}\check{\mathbf{H}}\hat{x} - \mathbf{K}\mathbf{H}x. \tag{18}$$

By adding and subtracting $\mathbf{K}\check{\mathbf{H}}x$, we get

$$\begin{aligned}\dot{\tilde{x}} &= \mathbf{F}\tilde{x} + \mathbf{K}\check{\mathbf{H}}\hat{x} - \mathbf{K}\mathbf{H}x + \mathbf{K}\check{\mathbf{H}}x - \mathbf{K}\check{\mathbf{H}}x \\ &= (\mathbf{F} - \mathbf{K}\check{\mathbf{H}})\tilde{x} + \mathbf{K}(\check{\mathbf{H}} - \mathbf{H})x = (\mathbf{F} - \mathbf{K}\check{\mathbf{H}})\tilde{x} + d(t)\end{aligned} \tag{19}$$

where

$$d(t) = \mathbf{K}(\check{\mathbf{H}} - \mathbf{H})x.$$

Since it is assumed that the pair $(\mathbf{F}, \check{\mathbf{H}})$ is UCO, it follows from standard KF theory that the origin of the nominal error dynamics (19) with $d = 0$ is GES. It is assumed that $||d(t)|| \leq k_d||\tilde{z}(t)||^2$ for some $k_d > 0$. Since k_d is bounded and does not depend on $\tilde{x}$, it follows from [47, Th. 2.1 and Proposition 2.3] that the equilibrium point $(\tilde{z}, \tilde{x}) = (0, 0)$ of the error dynamics of the cascade is also GES.

Appendix C
Proof of Lemma 5

The approach for showing UCO and UCC is using the algebraic transformations to simplify the measurement equations. As described in [29], it is possible to transform $[\rho_1 \cdots \rho_N, z]^T$

into $[\mathbf{p}^{n\,T}, \beta]^T$. Furthermore, it is shown in [2] how to transform, with a known position and β, $[\delta_{1,1} \cdots \delta_{N,M}]^T$ into two or more vectors in the NED frame. Two or more nonparallel vectors known in the body frame and measured in the NED frame can be used to fully determine attitude [17]. Consequently, if Assumptions 1 and 2 are fulfilled, the Jacobian of $[\delta_{1,1} \cdots \delta_{N,M}]^T$ w.r.t. $\mathbf{\Theta}$ will have full rank, and $[\delta_{1,1} \cdots \delta_{N,M}]^T$ is simplified as a 3-D vector function $\mathbf{f}_s$ in which the Jacobian w.r.t. $\mathbf{\Theta}$ will have full rank. The simplified measurement model can now be written as

$$\mathbf{h}(\chi) = \begin{bmatrix} \mathbf{p}^n \\ \beta \\ \mathbf{f}_s(\mathbf{p}^n, \beta, \mathbf{\Theta}) \\ -\mathbf{R}_n^b(\mathbf{\Theta})\mathbf{g}^n + \mathbf{b}_a \end{bmatrix}. \tag{20}$$

For an LKF to be applied, the model is linearized around the exogenous linearization point $\bar{\chi}$

$$\dot{\chi} = \mathbf{f}(\chi) = \mathbf{f}(\bar{\chi}) + \mathbf{F}(t)(\chi - \bar{\chi}) + \mathbf{G}(t)\epsilon_\chi + \gamma_\chi(t) \tag{21}$$

$$\mathbf{h}(\chi) = \mathbf{h}(\bar{\chi}) + \mathbf{H}(t)(\chi - \bar{\chi}) + \epsilon_h + \gamma_h(t) \tag{22}$$

where $\gamma_\chi(t)$ and $\gamma_h(t)$ are the linearization errors. To show UCO and UCC, it is not necessary to know $\mathbf{F}(t)$, $\mathbf{G}(t)$, and $\mathbf{H}(t)$ fully. However, the structure of the matrices is important, and some parts of the matrices are needed explicitly. For simplicity, the state is rearranged, such that $\chi = [\mathbf{p}^{n\,T}, \beta, \mathbf{b}_a^T, \mathbf{\Theta}^T, \mathbf{v}^{n\,T}, \mathbf{b}_\omega^T]^T$, and we define the process noise vector as $\epsilon_\chi = [\epsilon_\beta, \epsilon_{b_a}^T, \epsilon_\omega^T, \epsilon_a^T, \epsilon_{b_\omega}^T]^T$. It is possible to write

$$\mathbf{F}(t) = \left.\frac{\mathrm{d}\mathbf{f}(\chi)}{\mathrm{d}\chi}\right|_{\chi=\bar{\chi}} = \begin{bmatrix} \mathbf{0}_3 & \mathbf{0}_{3x1} & \mathbf{0}_3 & \mathbf{0}_3 & \mathbf{I}_3 & \mathbf{0}_3 \\ \mathbf{0}_{1x3} & 0 & \mathbf{0}_{1x3} & \mathbf{0}_{1x3} & \mathbf{0}_{1x3} & \mathbf{0}_{1x3} \\ \mathbf{0}_3 & \mathbf{0}_{3x1} & \mathbf{0}_3 & \mathbf{0}_3 & \mathbf{0}_3 & \mathbf{0}_3 \\ \mathbf{0}_3 & \mathbf{0}_{3x1} & \mathbf{0}_3 & \mathbf{A}_1 & \mathbf{0}_3 & -\mathbf{T} \\ \mathbf{0}_3 & \mathbf{0}_{3x1} & -\mathbf{R} & \mathbf{A}_2 & \mathbf{0}_3 & \mathbf{0}_3 \\ \mathbf{0}_3 & \mathbf{0}_{3x1} & \mathbf{0}_3 & \mathbf{0}_3 & \mathbf{0}_3 & \mathbf{0}_3 \end{bmatrix} \tag{23}$$

$$\mathbf{G}(t) = \left.\frac{\mathrm{d}\mathbf{f}(\chi)}{\mathrm{d}\epsilon_\chi}\right|_{\chi=\bar{\chi}} = \left[\begin{array}{ccccc} \mathbf{0}_{3x1} & \mathbf{0}_3 & \mathbf{0}_3 & \mathbf{0}_3 & \mathbf{0}_3 \\ \hline 1 & \mathbf{0}_{1x3} & \mathbf{0}_{1x3} & \mathbf{0}_{1x3} & \mathbf{0}_{1x3} \\ \mathbf{0}_{3x1} & \mathbf{I}_3 & \mathbf{0}_3 & \mathbf{0}_3 & \mathbf{0}_3 \\ \mathbf{0}_{3x1} & \mathbf{0}_3 & -\mathbf{T} & \mathbf{0}_3 & \mathbf{0}_3 \\ \mathbf{0}_{3x1} & \mathbf{0}_3 & \mathbf{0}_3 & -\mathbf{R} & \mathbf{0}_3 \\ \mathbf{0}_{3x1} & \mathbf{0}_3 & \mathbf{0}_3 & \mathbf{0}_3 & \mathbf{I}_3 \end{array}\right] \tag{24}$$

$$\mathbf{H}(t) = \left.\frac{\mathrm{d}\mathbf{h}(\chi)}{\mathrm{d}\chi}\right|_{\chi=\bar{\chi}} = \left[\begin{array}{cccc|cc} \mathbf{I}_3 & \mathbf{0}_{3x1} & \mathbf{0}_3 & \mathbf{0}_3 & \mathbf{0}_3 & \mathbf{0}_3 \\ \mathbf{0}_{1x3} & 1 & \mathbf{0}_{1x3} & \mathbf{0}_{1x3} & \mathbf{0}_{1x3} & \mathbf{0}_{1x3} \\ \mathbf{A}_3 & \mathbf{a}_1 & \mathbf{0}_3 & \mathbf{M} & \mathbf{0}_3 & \mathbf{0}_3 \\ \mathbf{0}_3 & \mathbf{0}_{3x1} & \mathbf{I}_3 & \mathbf{A}_4 & \mathbf{0}_3 & \mathbf{0}_3 \end{array}\right] \tag{25}$$

where $\mathbf{T}$ is given in (10) and $\mathbf{R}$ is defined in Section II-B (variable dependence have been removed for simplicity), $\mathbf{A}_{1,\ldots,4}$ are unknown 3×3 matrices, $\mathbf{a}_1$ is an unknown 3×1 vector, and $\mathbf{M}$ is a 3×3 matrix with full rank.

It is stated in [48] that the pair $(\mathbf{F}(t), \mathbf{H}(t))$ is UCO if the observability codistribution is given by

$$\mathrm{d}\mathcal{O} = \begin{bmatrix} M_0(t, \hat{\chi}) \\ \vdots \\ M_{n-1}(t, \hat{\chi}) \end{bmatrix} \tag{26}$$

has full rank for all t, where

$$M_0(t, \hat{\chi}) = \mathbf{H}(t)$$

$$M_m(t, \hat{\chi}) = M_{m-1}(t, \hat{\chi})\mathbf{F}(t) + \frac{\mathrm{d}}{\mathrm{d}t}M_{m-1}(t, \hat{\chi})$$

for $m = 0, \ldots, n-1$, where n is the state-space dimension. If the observability codistribution for $m = 0, 1$ has full rank, the full observability codistribution will also have full rank. It can be found from [49] that for the matrix

$$\mathrm{d}\mathcal{O} = \begin{bmatrix} M_0(t, \hat{\chi}) \\ M_1(t, \hat{\chi}) \end{bmatrix} = \begin{bmatrix} \mathcal{O}_1 & \mathbf{0}_{10x6} \\ \mathcal{O}_2 & \mathcal{O}_3 \end{bmatrix}$$

$\mathrm{rank}(\mathrm{d}\mathcal{O}) \geq \mathrm{rank}(\mathcal{O}_1) + \mathrm{rank}(\mathcal{O}_3)$.

$\mathcal{O}_1$ is defined as the part of $\mathbf{H}$ left of the dividing line in (25). By using the top four rows to remove $\mathbf{A}_3$ and $\mathbf{a}_1$, it can be shown that $\mathcal{O}_1$ has full rank, i.e., $\mathrm{rank}(\mathcal{O}_1) = 10$. $\mathcal{O}_3$ is given by

$$\mathcal{O}_3 = \begin{bmatrix} \mathbf{I}_3 & \mathbf{0}_3 \\ \mathbf{0}_{1x3} & \mathbf{0}_{1x3} \\ \mathbf{A}_3 & -\mathbf{MT} \\ \mathbf{0}_3 & -\mathbf{A}_4\mathbf{T} \end{bmatrix}. \tag{27}$$

Left or right multiplication by a nonsingular matrix leaves rank unchanged [50]. We define

$$\Pi = \{\pi/2 + k\pi : \; k \in \mathbb{Z}\}. \tag{28}$$

As $\mathbf{T}(\bar{\chi})$ is created from inverting $\mathbf{T}^{-1}(\bar{\chi})$, $\mathbf{T}(\bar{\chi})$ will be nonsingular and have full rank for $\theta \notin \Pi$, thus $\mathrm{rank}(\mathbf{MT}) = \mathrm{rank}(\mathbf{M}) = 3$ for $\theta \notin \Pi$. Consequently, by using the top three rows to remove $\mathbf{A}_3$, it can be shown that $\mathrm{rank}(\mathcal{O}_3) = 6$. If $\mathrm{rank}(\mathcal{O}_1) = 10$ and $\mathrm{rank}(\mathcal{O}_3) = 6$ for $\theta \notin \Pi$, then $\mathrm{rank}(\mathrm{d}\mathcal{O}) = 16$ for $\theta \notin \Pi$, proving that the system is UCO for $\theta \notin \Pi$.

It is stated in [48] that the pair $(\mathbf{F}(t), \mathbf{G}(t))$ is UCC if the controllability codistribution given by

$$\mathrm{d}\mathcal{C} = \begin{bmatrix} M_0(t, \hat{\chi}) & \cdots & M_{n-1}(t, \hat{\chi}) \end{bmatrix} \tag{29}$$

has full rank for all t, where

$$M_0(t,\hat{\chi}) = \mathbf{G}(t)$$

$$M_m(t,\hat{\chi}) = \mathbf{F}(t)M_{m-1}(t,\hat{\chi}) + \frac{\mathrm{d}}{\mathrm{d}t}M_{m-1}(t,\hat{\chi})$$

for $m = 0,\ldots,n-1$, where n is the state-space dimension. The same approach as for UCO can be applied, in which we look at

$$\mathrm{d}\mathcal{C} = \begin{bmatrix} M_0(t,\hat{\chi}) & M_1(t,\hat{\chi}) \end{bmatrix} = \begin{bmatrix} \mathbf{0}_{3x13} & \mathcal{C}_3 \\ \mathcal{C}_1 & \mathcal{C}_2 \end{bmatrix} \tag{30}$$

and $\mathrm{rank}(\mathrm{d}\mathcal{C}) \geq \mathrm{rank}(\mathcal{C}_1) + \mathrm{rank}(\mathcal{C}_3)$.

$\mathcal{C}_1$ is defined as the part of $\mathbf{G}$ under the dividing line in (24). As $\mathbf{R}$ is always invertible, it has full rank. It is clear from (24) that if $\mathbf{R}$ and $\mathbf{T}$ have full rank, $\mathrm{rank}(\mathcal{C}_1) = 13$ for $\theta \notin \Pi$. Furthermore, $\mathcal{C}_3$ is given by

$$\mathcal{C}_3 = \begin{bmatrix} \mathbf{0}_{3x1} & \mathbf{0}_3 & \mathbf{0}_3 & -\mathbf{R} & \mathbf{0}_3 \end{bmatrix}.$$

As $\mathbf{R}$ has full rank, $\mathrm{rank}(\mathcal{C}_3) = 3$. If $\mathrm{rank}(\mathcal{C}_1) = 13$ for $\theta \notin \Pi$ and $\mathrm{rank}(\mathcal{C}_3) = 3$, then $\mathrm{rank}(\mathrm{d}\mathcal{C}) = 16$ for $\theta \notin \Pi$, proving the system is UCC for $\theta \notin \Pi$.

ACKNOWLEDGMENT

The authors would like to thank their colleague B. Stovner for being an equal part in developing the ranging algorithm for use with the Waterlinked acoustic system.

REFERENCES

[1] E. K. Jørgensen and I. Schjølberg, "Attitude and gyro bias estimation using range-difference and IMU measurements," in *Proc. IEEE/OES Auton. Underwater Veh.*, 2016, pp. 124–130.

[2] E. K. Jørgensen and I. Schjølberg, "Attitude and rate sensor bias estimation for underwater vehicles," in *Proc. 26th Mediterranean Conf. Control Autom.*, 2018, pp. 1–7.

[3] B. Vik, "Integrated satellite and inertial navigation systems," Dept. Eng. Cybern., Norwegian Univ. Sci. Technol., Trondheim, Norway, TTK5 Lecture Notes, 2009.

[4] C. E. Cohen, B. W. Parkinson, and B. D. McNally, "Flight tests of attitude determination using GPS compared against an inertial navigation unit," *Navigation*, vol. 41, no. 1, pp. 83–97, 1994.

[5] J. Yan, C. C. Tiberius, G. J. Janssen, P. J. Teunissen, and G. Bellusci, "Review of range-based positioning algorithms," *IEEE Aerosp. Electron. Syst. Mag.*, vol. 28, no. 8, pp. 2–27, Aug. 2013.

[6] P. Batista, "GES long baseline navigation with unknown sound velocity and discrete-time range measurements," *IEEE Trans. Control Syst. Technol.*, vol. 23, no. 1, pp. 219–230, Jan. 2015.

[7] P. Batista, "Long baseline navigation with clock offset estimation and discrete-time measurements," *Control Eng. Pract.*, vol. 35, pp. 43–53, 2015.

[8] P. Batista, C. Silvestre, and P. Oliveira, "Sensor-based long baseline navigation: Observability analysis and filter design," *Asian J. Control*, vol. 16, no. 4, pp. 974–994, 2014.

[9] M. Bayat, N. Crasta, A. P. Aguiar, and A. M. Pascoal, "Range-based underwater vehicle localization in the presence of unknown ocean currents: Theory and experiments," *IEEE Trans. Control Syst. Technol.*, vol. 24, no. 1, pp. 122–139, Jan. 2016.

[10] D. De Palma, F. Arrichiello, G. Parlangeli, and G. Indiveri, "Underwater localization using single beacon measurements: Observability analysis for a double integrator system," *Ocean Eng.*, vol. 142, pp. 650–665, 2017.

[11] G. Vallicrosa and P. Ridao, "Sum of Gaussian single beacon range-only localization for AUV homing," *Annu. Rev. Control*, vol. 42, pp. 177–187, 2016.

[12] J. Vaganay, J. G. Bellingham, and J. J. Leonard, "Comparison of fix computation and filtering for autonomous acoustic navigation," *Int. J. Syst. Sci.*, vol. 29, no. 10, pp. 1111–1122, 1998.

[13] B. Bell, B. Howe, J. Mercer, and R. Spindel, "Nonlinear Kalman filtering of long-baseline, short-baseline, GPS, and depth measurements," in *Proc. Conf. Rec. 25th Asilomar Conf. Signals, Syst. Comput.*, 1991, pp. 131–136.

[14] A. Alcocer, P. Oliveira, and A. Pascoal, "Study and implementation of an EKF GIB-based underwater positioning system," *Control Eng. Pract.*, vol. 15, no. 6, pp. 689–701, 2007.

[15] J. C. Kinsey and L. L. Whitcomb, "Preliminary field experience with the DVLNAV integrated navigation system for oceanographic submersibles," *Control Eng. Pract.*, vol. 12, no. 12, pp. 1541–1549, 2004.

[16] L. L. Whitcomb, D. R. Yoerger, H. Singh, and J. Howland, "Combined Doppler/LBL based navigation of underwater vehicles," in *Proc. 11th Int. Symp. Unmanned Untethered Submersible Technol.*, 1999, vol. 9818.

[17] M. D. Shuster and S. D. Oh, "Three-axis attitude determination from vector observations," *J. Guid., Control, Dyn.*, vol. 4, no. 1, 2012, Art. no. AIAA 81-4003.

[18] R. Mahony, T. Hamel, and J.-M. Pflimlin, "Nonlinear complementary filters on the special orthogonal group," *IEEE Trans. Autom. Control*, vol. 53, no. 5, pp. 1203–1217, Jun. 2008.

[19] H. F. Grip, T. I. Fossen, T. A. Johansen, and A. Saberi, "Attitude estimation using biased gyro and vector measurements with time-varying reference vectors," *IEEE Trans. Autom. Control*, vol. 57, no. 5, pp. 1332–1338, May 2012.

[20] F. L. Markley *et al.*, "Attitude error representations for Kalman filtering," *J. Guid. Control Dyn.*, vol. 26, no. 2, pp. 311–317, 2003.

[21] A. M. Sabatini, "Quaternion-based extended Kalman filter for determining orientation by inertial and magnetic sensing," *IEEE Trans. Biomed. Eng.*, vol. 53, no. 7, pp. 1346–1356, Jul. 2006.

[22] S. Salcudean, "A globally convergent angular velocity observer for rigid body motion," *IEEE Trans. Autom. Control*, vol. 36, no. 12, pp. 1493–1497, Dec. 1991.

[23] J. L. Crassidis, F. L. Markley, and Y. Cheng, "Survey of nonlinear attitude estimation methods," *J. Guid., Control, Dyn.*, vol. 30, no. 1, pp. 12–28, 2007.

[24] P. Batista, C. Silvestre, P. Oliveira, and B. Cardeira, "Accelerometer calibration and dynamic bias and gravity estimation: Analysis, design, and experimental evaluation," *IEEE Trans. Control Syst. Technol.*, vol. 19, no. 5, pp. 1128–1137, Sep. 2011.

[25] S.-H. P. Won and F. Golnaraghi, "A triaxial accelerometer calibration method using a mathematical model," *IEEE Trans. Instrum. Meas.*, vol. 59, no. 8, pp. 2144–2153, Aug. 2010.

[26] H. F. Grip, T. I. Fossen, T. A. Johansen, and A. Saberi, *Multisensor Attitude Estimation*. Boca Raton, FL, USA: CRC Press, 2016, ch. 17, pp. 291–314.

[27] J. Farrell, *Aided Navigation: GPS With High Rate Sensors*. New York, NY, USA: McGraw-Hill, 2008.

[28] P. Batista, C. Silvestre, and P. Oliveira, "GES integrated LBL/USBL navigation system for underwater vehicles," in *Proc. IEEE 51st IEEE Conf. Decis. Control*, 2012, pp. 6609–6614.

[29] E. K. Jørgensen, T. A. Johansen, and I. Schjølberg, "Enhanced hydroacoustic range robustness of three-stage position filter based on long baseline measurements with unknown wave speed," *IFAC-ArticlesOnLine*, vol. 49, no. 23, pp. 61–67, 2016.

[30] E. K. Jørgensen, B. B. Stovner, and I. Schjølberg, "Experimental validation of three-stage position filter based on long baseline measurements with unknown wave speed," in *Proc. IEEE Conf. Control Technol. Appl.*, 2017, pp. 680–686.

[31] T. A. Johansen and T. I. Fossen, "The exogenous Kalman filter (XKF)," *Int. J. Control*, vol. 90, no. 2, pp. 161–167, 2017.

[32] T. A. Johansen and T. I. Fossen, "Nonlinear filtering with exogenous Kalman filter and double Kalman filter," in *Proc. Eur. Control Conf.*, 2016, pp. 1722–1727.

[33] B. Ristic, S. Arulampalam, and N. Gordon, "Beyond the Kalman filter—Book review," *IEEE Aerosp. Electron. Syst. Mag.*, vol. 19, no. 7, pp. 37–38, Jul. 2004.

[34] F. Gustafsson, *Statistical Sensor Fusion*. Lund, Sweden: Studentlitteratur, 2010.

[35] T. I. Fossen, *Handbook of Marine Craft Hydrodynamics and Motion Control*. Hoboken, NJ, USA: Wiley, 2011.

[36] J. B. Kuipers *et al.*, *Quaternions and Rotation Sequences*, vol. 66. Princeton, NJ, USA: Princeton Univ. Press, 1999.

[37] B. B. Stovner, T. A. Johansen, T. I. Fossen, and I. Schjølberg, "Three-stage filter for position and velocity estimation from long baseline measurements with unknown wave speed," in *Proc. Amer. Control Conf.*, 2016, pp. 4532–4538.

[38] "Waterlinked webpage," Accessed: Jul. 1, 2017. [Online]. Available: https://waterlinked.com/

[39] M. S. Grewal, L. R. Weill, and A. P. Andrews, *Global Positioning Systems, Inertial Navigation, and Integration*. Hoboken, NJ, USA: Wiley, 2007.
[40] T. H. Bryne, J. M. Hansen, R. H. Rogne, N. Sokolova, T. I. Fossen, and T. A. Johansen, "Nonlinear observers for integrated INS/GNSS navigation: Implementation aspects," *IEEE Control Syst.*, vol. 37, no. 3, pp. 59–86, Jun. 2017.
[41] J. M. Hansen, T. I. Fossen, and T. A. Johansen, "Nonlinear observer design for GNSS-aided inertial navigation systems with time-delayed gnss measurements," *Control Eng. Pract.*, vol. 60, pp. 39–50, 2017.
[42] Y. Bar-Shalom, *Tracking and Data Association*. New York, NY, USA: Academic, 1987.
[43] G. Indiveri, D. De Palma, and G. Parlangeli, "Single range localization in 3-D: Observability and robustness issues," *IEEE Trans. Control Syst. Technol.*, vol. 24, no. 5, pp. 1853–1860, Sep. 2016.
[44] E. Olson, J. J. Leonard, and S. Teller, "Robust range-only beacon localization," *IEEE J. Ocean. Eng.*, vol. 31, no. 4, pp. 949–958, Oct. 2006.
[45] J. Jouffroy and J. Opderbecke, "Underwater vehicle navigation using diffusion-based trajectory observers," *IEEE J. Ocean. Eng.*, vol. 32, no. 2, pp. 313–326, Apr. 2007.
[46] H. F. Grip, T. I. Fossen, T. A. Johansen, and A. Saberi, "Globally exponentially stable attitude and gyro bias estimation with application to GNSS/INS integration," *Automatica*, vol. 51, pp. 158–166, 2015.
[47] A. Loría and E. Panteley, "Cascaded nonlinear time-varying systems: Analysis and design," in *Advanced Topics in Control Systems Theory*. New York, NY, USA: Springer, 2005, ch. 2, pp. 23–64.
[48] C.-T. Chen, *Linear System Theory and Design*. London, U.K.: Oxford Univ. Press, 1995.
[49] C. D. Meyer, Jr, "Generalized inverses and ranks of block matrices," *SIAM J. Appl. Math.*, vol. 25, no. 4, pp. 597–602, 1973.
[50] R. A. Horn and C. R. Johnson, *Matrix Analysis*. Cambridge, U.K.: Cambridge Univ. Press, 2012.